Magnetic resonance imaging and spectroscopy of intracranial tuberculomas

Rakesh K. Gupta*,† and Raja Roy
*MR Section, Department of Radiology, Sanjay Gandhi Post-Graduate Institute of Medical Sciences, Lucknow 226 014, India
Regional Sophisticated Instrumentation Centre, Central Drug Research Institute, Lucknow 226 014, India

The incidence of intracranial tuberculomas is on the rise both in developed and developing countries. Differentiation of tuberculomas from other neoplastic and non-neoplastic lesions is essential. In this article, we review the application of MR imaging and spectroscopy in tissue characterization of intracranial tuberculomas.

INTRACRANIAL tuberculomas account for 20–40% of the intracranial space occupying mass lesions in the developing countries. The incidence of tuberculomas is on the rise even in the developed countries due to the pandemic of HIV. Differentiation of tuberculomas from other neoplastic and non-neoplastic lesions is essential as tuberculomas can be managed conservatively with antituberculous drugs and unnecessary surgical intervention can be avoided. CT and MRI are the imaging techniques usually used in the anatomical localization and characterization of such lesions. MRI is considered superior to CT for better localization and characterization of intracranial tuberculomas[1,2].

In vivo magnetic resonance spectroscopy (MRS) is a novel, non-invasive, powerful technique that can give biochemical information of the patho-physiological process of the tissue in question. The technique has been used in differentiation of neoplastic from inflammatory intracranial masses[3]. The lesions, which may have similar imaging features with different pathological process, can be distinguished by *in vivo* MRS. In this paper we summarize the application of MRI and MRS in tissue characterization of intracranial tuberculomas.

MRI

Intracranial tuberculomas may occur with or without meningitis and is usually present as either solitary or multiple tuberculomas formation[4,5]. These lesions originate as a conglomerate of microgranulomata in an area of tuberculous cerebritis that join to form a noncaseating tuberculoma. In most cases, subsequent central caseous necrosis develops that is initially solid but in some instances may eventually liquefy[6]. The MR features of the individual tuberculoma depend on whether the granuloma is noncaseating or caseating with a solid centre, or caseating with a liquid center[7,8].

The noncaseating granuloma is usually iso/hypointense on T_1- and hyperintense on T_2-weighted images[7,8]. These granulomas show homogeneous enhancement after injection of paramagnetic contrast agent. The caseating solid granulomas appear relatively iso/hypointense on T_1-weighted images and isointense to hypointense on T_2-weighted images (Figure 1 *a*). The lesions which are not visible (isointense on both T_1 and T_2-weighted images) on conventional spin echo images, and either enhance after contrast administration or become visible on magnetization transfer contrast images are, referred to as conventional spin echo invisible lesions[8] (Figure 1 *b*). The degree of hypointensity of the solid caseating granuloma on T_2-weighted images depends on the complex relationship between the solid caseation, associated regional fibrosis/gliosis, macrophage infiltration and macrophage by-products like the release of free radicals, and perilesional cellular infiltrate[7]. Physically, the caseous material is 'cheesy' in texture and is relatively high in lipid content[7]. The granulomas are typically associated with variable degree of surrounding oedema that is relatively hypointense on T_1-weighted images and hyperintense on T_2-weighted images; the wall of the caseating tuberculous granuloma often shows a striking hypointense rim on T_2-weighted images. Gadolinium-enhanced T_1-weighted images show rim enhancement in such caseating lesions[4,8].

The granulomas with central liquefaction of the caseous material appear centrally hypointense on T_1- and hyperintense on T_2-weighted images with a peripheral hypointense rim on T_2-weighted images. In such cases, the hypointense rim represents the tuberculoma capsule. The images acquired after intravenous gadolinium administration in these cases also show rim enhancement. These latter lesions may be indistinguishable on MR from true tuberculous or pyogenic abscess formation[8]. Pathologically the caseating tubercle contains only rare tubercular organisms, but the tuberculous abscess has a semi liquid centre teeming with tubercular bacilli. Parenchymal tuberculous granulomas or abscesses can be seen in the brain, spinal cord and/or in association with the leptomeninges and may be solitary, multiple or miliary in distribution.

†For correspondence. (e-mail: rakeshree@hotmail.com)

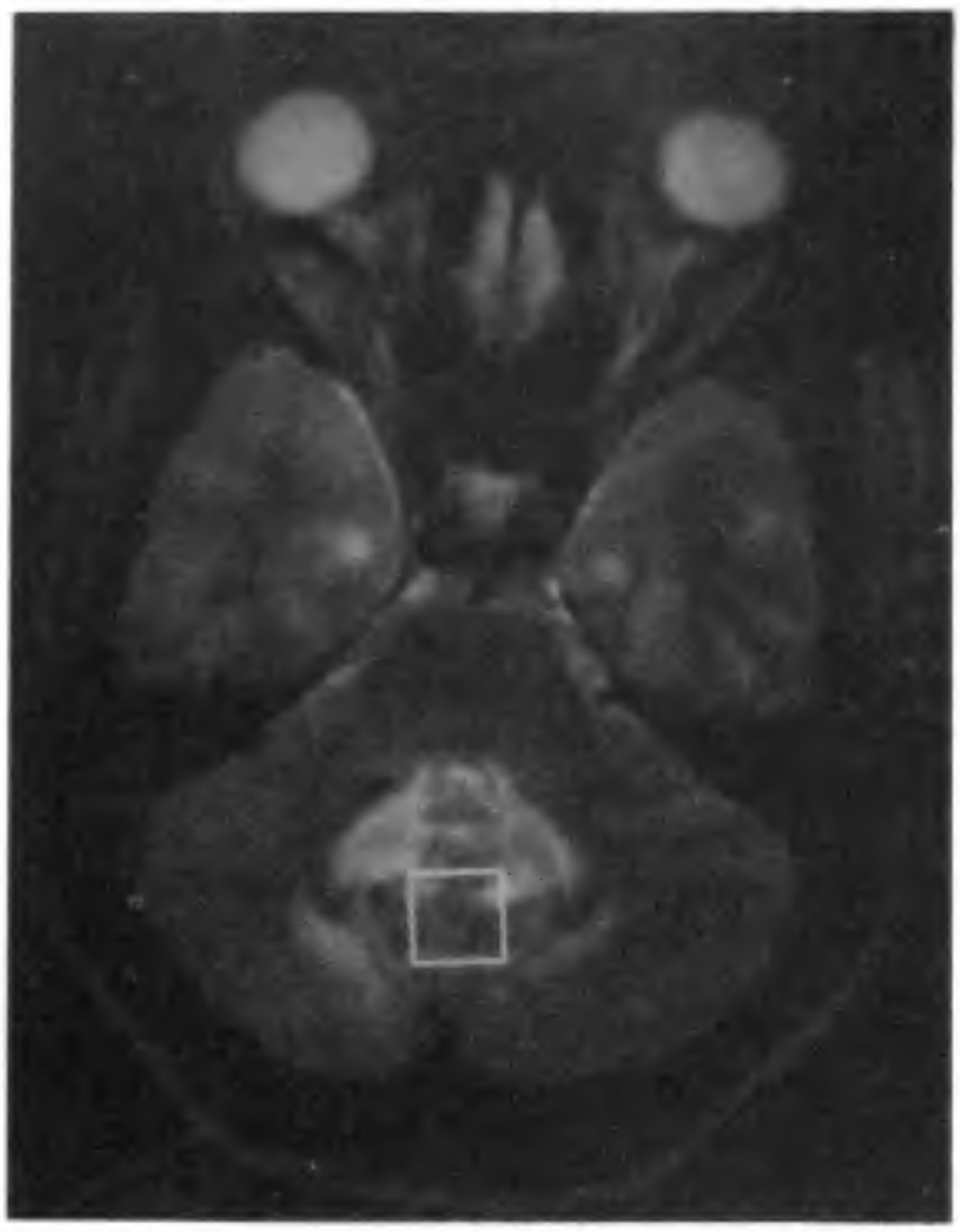

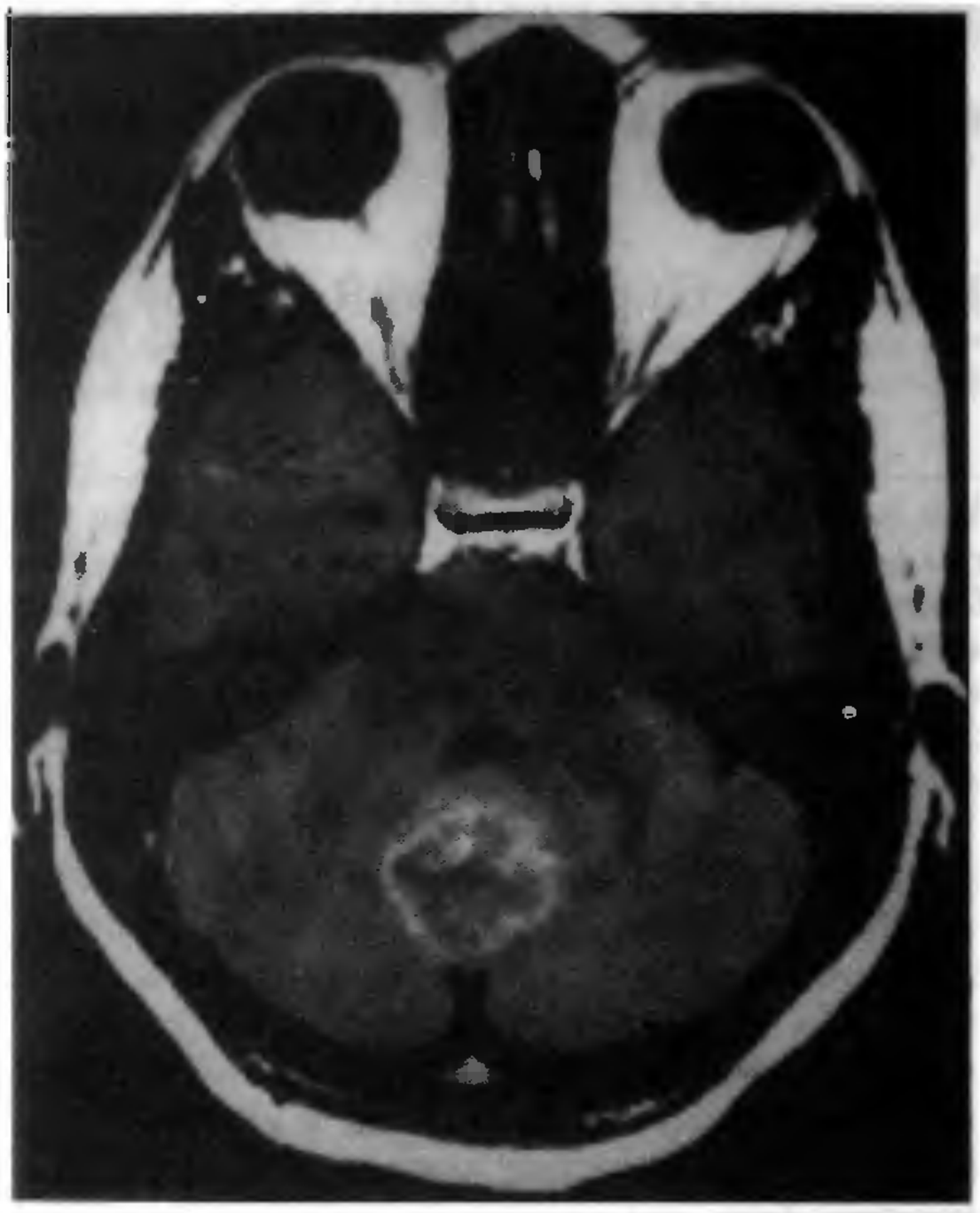

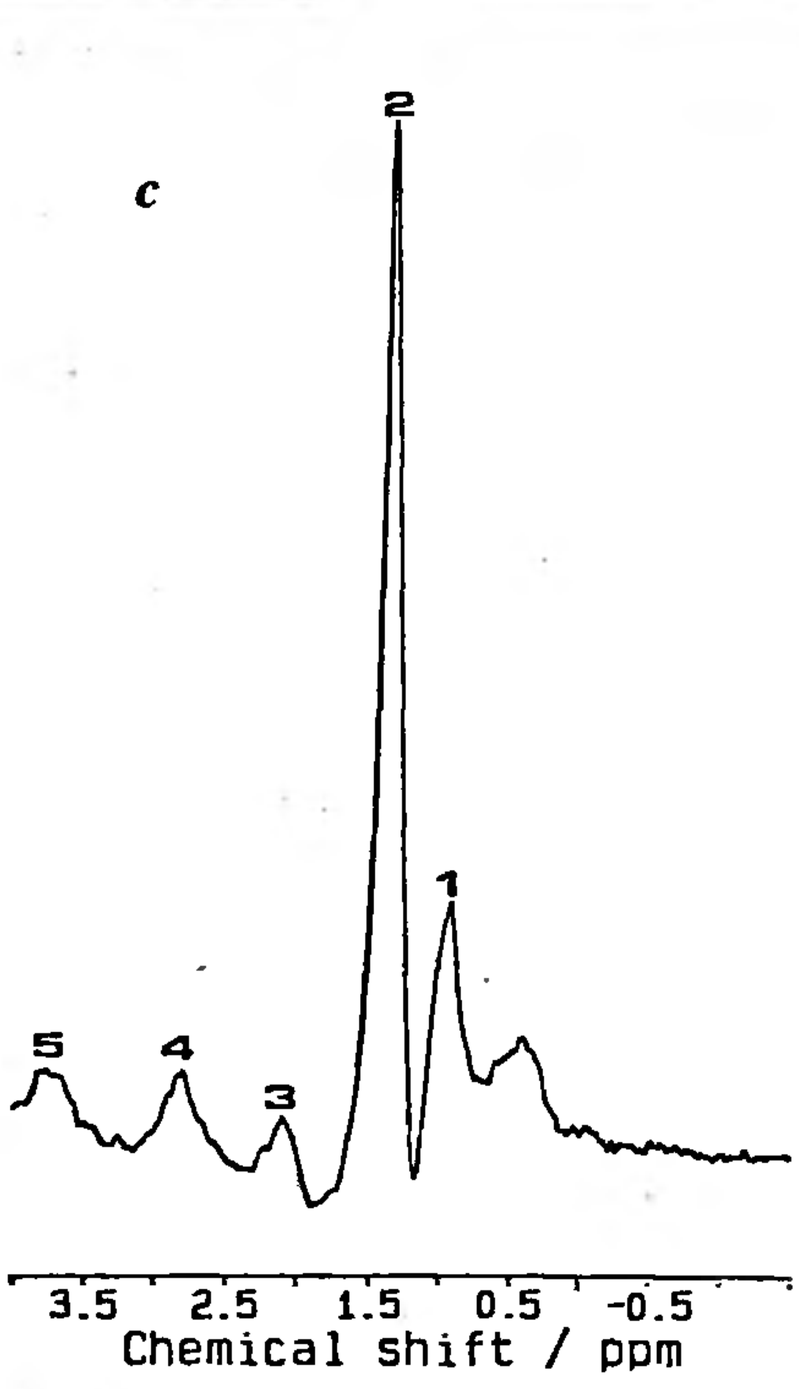

Figure 1. Vermian tuberculoma; *a*, *b*, T_2-weighted axial image through the cerebellum; *a*, Hypointense mass in the vermis with hyperintense perifocal oedema. The mass is better defined on MT-SE T_1-weighted image; *b*. Inset in *a* shown is the volume of interest from where *in vivo* proton MR spectrum was obtained; *c*, Proton MR spectrum using STEAM sequence (TE = 20 m sec) from the tuberculoma shows different resonances (1, $-CH_3$; 2, $(CH_2)_n$; 3, $H_2C{=}CH$; 4, $CH\text{-}CH_2CH{=}$; 5, Phosphoserine).

The capsules of caseating tuberculous lesions and the whole of noncaseating lesions show evidence of microscopic hypervascularity as determined by sensitive imaging techniques (dynamic bolus contrast enhanced CT). Therefore, inflammatory neovascularity seems to be responsible both for this hypervascularity and for part of the enhancement observed after contrast agent administration[8] (i.e. blood–brain barrier disruption caused by leaky neovessels).

Miliary brain tuberculosis usually is associated with tuberculous meningitis, although it may be asymptomatic with pulmonary miliary tuberculosis or may precede meningitis[5,8,9]. Miliary tubercles are less than 2 mm and are either not visible on conventional spin echo MR images or show tiny foci of hyperintensity on T_2-weighted acquisitions. T_1-weighted images after gadolinium administration show numerous round, small, homogeneous enhancing lesions[9]. The spin echo invisible lesions, which may or may not enhance after intravenous injection of godolinium diamine trimethyl penta acetic acid (Gd-DTPA) are clearly visible on magnetization transfer spin echo (MT-SE) T_1-weighted imaging. MT-SE imaging helps in defining the true disease load as an individual granuloma may respond differently to antituberculous drugs.

It may be useful here to discuss the types of changes in appearance that have been observed within tuberculomas while the patient was receiving antituberculous therapy. In those receiving antituberculous treatment, there is a progressive decrease in the amount of oedema associated with a reduction in the overall size of the lesion[2,8]. If treatment is successful, the lesion may disappear altogether as judged by conventional MR. However the residual lesion or gliosis, which may not be visible on conventional spin echo imaging, may still show on MT-SE images. Nonenhancing residual encephalomalacia with or without calcification is also a sign of healing. Calcium deposits, when present, typically appear hypointense on T_1-, T_2- and T_2*-weighted images[8]. Only rarely has a paradoxical response been observed in which the increase in size of the lesion was seen, while the patient was on antituberculous therapy[2]. Nevertheless, these latter tuberculomas were seen to regress gradually with continued medical treatment.

As a general rule, different phenomena have been demonstrated concerning tuberculous lesions[8]: (1) different lesions in a single patient may be in a different stage of evolution at the time of initial diagnosis; (2) different lesions in the same patient may respond to medical therapy differently (i.e. resolve at different rates); (3) similar appearing lesions in different patients may respond to medical treatment differently; (4) larger centrally caseous lesions in any location in general take longer to resolve than smaller noncaseous lesions; (5) the larger the lesion is initially, the greater is the likelihood of permanent sequelae, (e.g. calcification, encephalomalacia).

MRS

In vivo proton MRS

In vivo proton MRS is a non-invasive technique, which has been utilized in the diagnosis and management of various intracranial abnormalities. Differentiation of neoplastic from infective intracranial mass lesions is possible with the help of the single voxel technique using different echo times[3]. *In vivo* spectra are found to be specific for intracranial tuberculomas when combined with imaging and demonstrate the biochemical fingerprints of the tubercle bacilli in a granuloma.

Technique

Single voxel and multi voxel approaches have been used by different workers in the spectroscopic evaluation of intracranial mass lesions. We use single voxel technique, stimulated echo acquisition mode (STEAM) and spin echo sequences. The *in vivo* spectroscopy experience in 55 surgically proven tuberculomas in this article is based on the single voxel technique. The typical volume selected varied between 4 and 8 ml. It was ensured that the lesion was big enough to have the voxel well within the lesion in all the slices where the lesion was seen. The parameters for the STEAM sequence used were TR/TE/TM/No. of acquisitions = 3000/20, 270/30/128 with acquisition time of 6.5 min for each echo time (TE); SE sequence with TR/TE/No of excitations = 3000/135/256 with acquisition time of 13 min. The SE sequence was used to look for the presence of *j*-coupled metabolites. After voxel shimming, the line width of the water resonance at full width half-maximum was typically 5 Hz. Post processing of the real part of the averaged free induction decay (FID) included zero filling to 4 k data points, followed by Gaussian multiplication, Fourier transformation, and phase correction. No baseline correction was done. Assignments of resonances seen *in vivo* were based on the existing literature at 1.5 tesla[3,10]. Resonances not assigned earlier on *in vivo* spectroscopy were assigned by performing *ex vivo* and *in vitro* studies of the excised tissue.

Resonances observed on in vivo MRS

Resonances were observed at 0.9, 1.3, 2.0, 2.8 and 3.7 ppm on STEAM 20-msec sequence (Figure 1 *c*). On SE 135 msec, resonances at 1.3 and 0.9 ppm showed marked reduction in signal intensity, while the rest of the resonances were barely visible. The resonances at 0.9, 1.3, 2.0, 2.8 and 3.7 ppm were assigned to terminal methyl (CH_3), acyl chain $(CH_2)_n$, CH_2=CH in fatty acyl chain, =CH-CH_2CH= in fatty acyl chain and phosphoserine respectively[11,12]. Neoplastic lesions show high choline, low to very low N-acetyl asparate (NAA) and

lactate and/or lipid and are clearly distinct from infective lesions. We had very consistent spectra in all the cases of tuberculomas so far studied on *in vivo* MRS. One of the close differential diagnoses of T_2 black lesion is healing cysticercus granuloma. Unfortunately, these lesions are usually less than 1 cm and cannot be cleanly studied with the current technique available here. There is no literature clearly showing the spectra in such lesions backed up by the *ex vivo* and *in vitro* study. Brain abscess shows acetate, pyruvate, leucine, isoleucine, valine, alanine, lipid, lactate, glycine and other amino acids that have not been described in other infective lesions and neoplasm on *in vivo* study[3].

Ex vivo and in vitro study

These techniques were used with the purpose of confirming the assignment of the resonances and to assess the utility of these techniques for better diagnosis and management of such lesions. The spectral resolution of *in vivo* MRS is relatively poor due to the low magnetic field used for clinical studies and low homogeneity.

Excised tissue (usually 2–3 g) was collected while the patient underwent surgery and snap frozen in liquid nitrogen.

Ex vivo study. About 3 × 3 × 4 mm of the excised tuberculoma tissue after thawing was placed in a 5 mm NMR tube containing a 1.5 cm column of agarose gel in its lowest part. D_2O was added for internal locking of the sample. *Ex vivo* study was performed at 37°C for a period of 4 h. The sample was then removed from the NMR tube and immersed immediately in 10% formalin solution, and was sent for histopathological examination.

In vitro study. The remaining sample was divided into two parts and perchloric acid (PCA) and lipid extraction was done using standard techniques. *In vitro* studies from the PCA and lipid extracts of *Mycobacterium tuberculosis* H37 Ra and Rv strains were done to compare and correlate the biochemicals of the bacteria with the granulomas.

High resolution MRS. All *ex vivo* and *in vitro* studies were performed on a 300 MHz spectrometer (Bruker Avance DRX, Switzerland), equipped with 5 mm multinuclear inverse probe head with *z* shielded gradient. All *ex vivo* and *in vitro* spectra were obtained at 37°C in a nonspinning mode. After optimization of the magnetic field homogeneity, the line width of water resonance was typically 14 Hz. One D spectrum was obtained by using two different sequences; a single pulse sequence with frequency selective water presaturation, and SE sequence for long T_2 components in the sample (TE ≈ 80 msec). Each spectrum was acquired with 32,768 data points in sequential mode and a spectral width of 3.591 kHz; 64 scans are averaged with a recycle delay of 3 s. Standard 2D correlation spectroscopy (COSY) 90° spectra were acquired with frequency selective water presaturation. The spectral width was 3.591 kHz in both dimensions; 256 t_1 increments in the 1.143 s recycle delay. For each t_1 step, 16 transients were added with 1024 data points. The total acquisition time was 4 h 20 min. The data were weighted with sine bell window function in both dimensions before double Fourier transformation. The final matrix was 1024 × 256 points.

Resonances observed on ex vivo, and in vitro study. Ex vivo single pulse spectrum showed resonances at 0.9, 1.3, 1.58, 2.02, 2.24, 2.80, 3.22, 3.79, 4.1, 4.29 and 5.33 ppm assigned to terminal methyl (CH_3), acyl chain $(CH_2)_n$, $OC\text{-}CH_2\text{-}CH_2$ in fatty acyl chain, $CH_2{=}CH$ in fatty acyl chain, $COCH_2$ in fatty acyl chain, $=CH\text{-}CH_2CH=$ in fatty acyl chain, $-N(CH_3)_3$ of choline, phosphoserine, glycerol backbone of phospholipids and olefinic group of lipids respectively[12–17] (Figure 2 *a*).

Spin echo Fourier transformed (SEFT) spectrum showed the phase reversal of resonances at 1.3 and 3.7 ppm to 3.8 ppm, assigned to lactate and serine (serine containing compounds, namely serine, phosphoserine, and phosphatidylserine), respectively. The sharp resonance at 2.29 ppm was assigned to acetoacetate. Terminal methyl at 0.9 ppm, acyl chain at 1.3 ppm and olefinic group at 5.3 ppm showed marked reduction in signal (Figure 2 *b*). Other resonances seen in single pulse spectrum were not visible in SEFT spectrum confirming that those resonances were due to the different lipids.

Ex vivo 2D COSY spectrum confirmed all the resonances seen on 1D single pulse and SEFT spectra. In addition, alanine (1.48 ppm, 3.76 ppm) and threonine (1.34 ppm, 4.25 ppm) were also observed (Figure 2 *c*).

The PCA and lipid extracts of tuberculoma and *M. tuberculosis* showed similarity of spectra. Besides lipids, which are usually seen in any tissue, the unusual resonances seen in granuloma at 0.5 and 0.1 ppm were assigned to cyclopropane rings and at 7.1 and 7.4 ppm assigned to phenolic lipids. These resonances were also observed in *M. tuberculosis* confirming the granuloma was of mycobacterial origin[12] (Figure 3 *a, b*). PCA extracts of tuberculoma showed leucine/valine (0.95 ppm), beta hydroxybutyrate (1.2 ppm), lactate (1.33, 4.1 ppm), acetate (1.92 ppm), glutamate (2.19 ppm), acetoacetate (2.29 ppm), lysine (3.46 ppm), serine (3.7–3.9 ppm), adenine (8.1, 8.4 ppm), guanine (8.2 ppm). The PCA extract of *M. tuberculosis* showed a small amount of serine confirmed by SEFT and 2D COSY study.

A number of *ex vivo* studies of different intracranial neoplastic lesions have shown high choline, lipids, lactate, and some amino acids[14]. These are dependent on

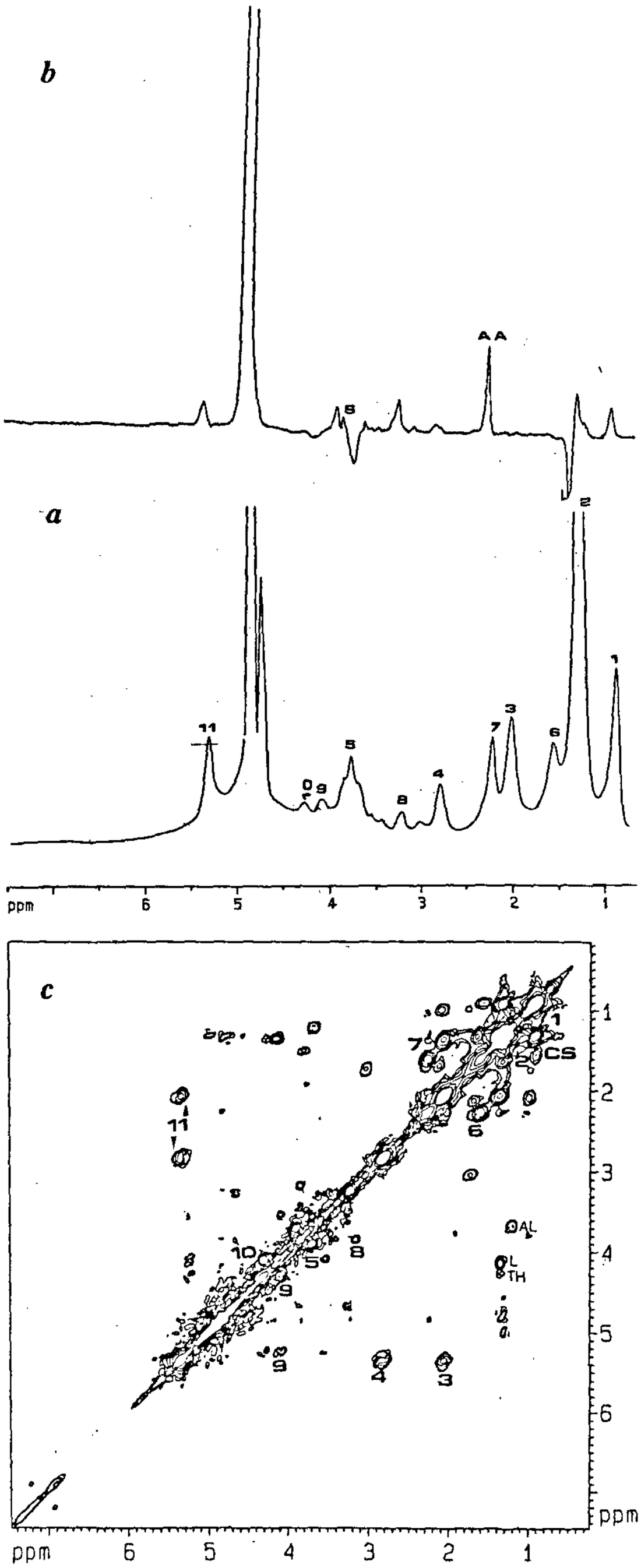

Figure 2. *Ex vivo* study; ***a***, *Ex vivo* single pulse spectrum of the excised tuberculoma shown in Figure 1 *a* (6, $OC\_CH_2\_CH_2$; 7, $OC\text{-}CH_2$; 8, choline; 9, phospholipids; 10, triglyceride back bone; 11, olifinic group; 1–5 as in Figure 1); ***b***, SEFT spectrum (TE = 80 msec) shows phase reversal of lactate (L) and serine (S) with acetoacetate (AA) at 2.29 ppm. Note the marked reduction or disappearance of various lipid resonances seen in *a*; ***c***, 2D COSY spectrum (AL, alanine; TH, threonine; CS, cholesterol; rest as in Figures 1, 2 *a*, *b*).

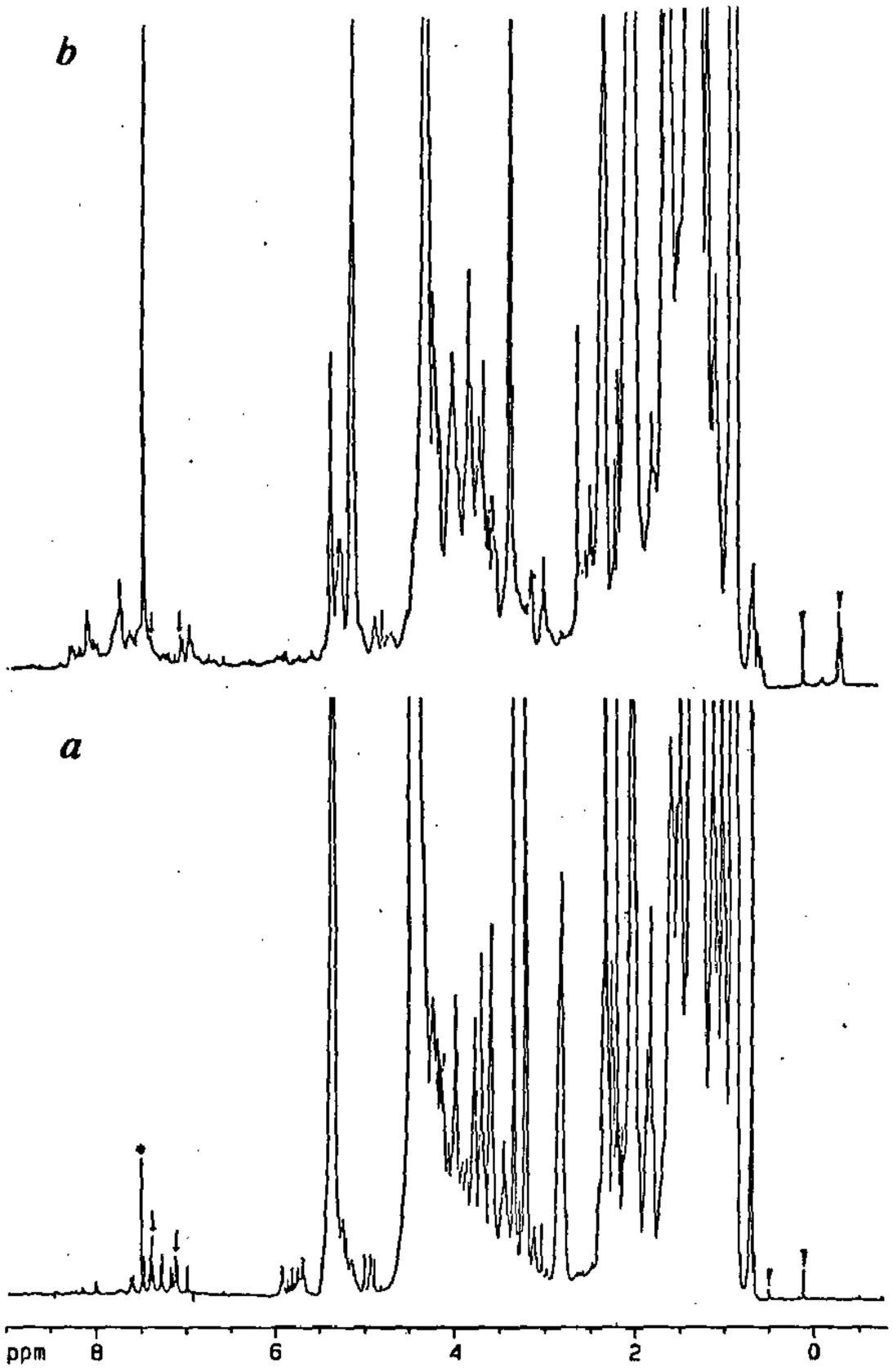

Figure 3. *In vitro* study; ***a***, Lipid extract of tuberculoma. Single pulse spectrum of the tuberculoma shows phenolic lipids (arrows) and cyclopropane rings (arrow heads). (*, $CHCl_3$, an external reference at 7.5 ppm in a mixture of $CDCl_3$:CD_3OD::3:1); ***b***, Lipid extract of *M. tuberculosis*. Single pulse spectrum of *M. tuberculosis* also shows similar resonances of cyclopropane rings (arrow heads) and phenolic lipids (arrows) seen in tuberculous granuloma.

the consistency of the mass lesions from where the spectrum is obtained. Presence of lipids suggests hypoxia along with micro/macronecrosis[14]. Granulomas show caseation necrosis and lipids were visible on *ex vivo* study[12]. However the presence of serine on *ex vivo/in vitro* study is distinct in tuberculomas and has not been observed so far in any other intracranial mass lesion[12]. One of the characteristic features of mycobacterium is presence of a lipid rich cell wall dominated by a wide variety of species and type-specific glycolipids[17]. Phenolic glycolipids are present in virulent and avirulent strains of different species of mycobacterium. Demonstration of phenolic glycolipids on *ex vivo/in vitro* study in tuberculomas suggests that phenolic lipids represent the constituents of cell wall of the living/dying or dead mycobacteria in a granuloma[12].

Tissue destruction leading to caseation is a particular feature of tuberculosis and is rarely found in other immunological and nonimmunological granulomas. Caseation is a cheese-like necrosis and is composed of necrosed tissue, inflammatory cells, and dead/fragmented/lysed mycobacteria. Presence of phenolic lipids represents the biochemical fingerprints of *M. tuberculosis* in a granuloma[12]. Isolation of *M. tuberculosis* from the tissue either on smear or culture is possible in a very small number of cases and diagnosis rests on demonstration of caseating granuloma on histology. In a significant number of cases, even caseation is not seen and it becomes difficult to differentiate tuberculous granuloma from other non-tuberculous granulomas[18]. Besides culture having a low yield, it takes about 6–8 weeks for the results; and treatment cannot be withheld for such a long time due to prognostic reasons[18]. Lipid extraction for the purpose of MRS is a relatively simple procedure and can be performed routinely in most well equipped laboratories. It may help as an additional tool in the fingerprinting of *M. tuberculosis* cell wall biochemicals in the granuloma and may help in facilitating the diagnosis, where routine histology and culture are not conclusive.

We conclude that MRI and MRS help in better tissue characterization of intracranial tuberculomas.

1. Gupta, R. K., Jena, A., Sharma, A., Guha, D., Khushu, S. and Gupta, A. K., *J. Comput. Assist. Tomogr.*, 1988, **12**, 280–285.
2. Gupta, R. K., Jena, A., Singh, A. K., Puri, V., Sharma, A. and Gupta, M., *Clin. Radiol.*, 1990, **41**, 120–127.
3. Poptani, H., Gupta, R. K., Roy, R., Pandey, R., Jain, V. K. and Chhabra, D. K., *Am. J. Neuroradiol.*, 1995, **16**, 1593–1603.
4. Chang, K. H., Han, M. H. and Roh, J. K., *Neuroradiology*, 1990, **32**, 19–25.
5. Gupta, R. K., Gupta, S., Singh, D., Kohli, A., Sharma, B. and Gujral, R. B., *Neuroradiology*, 1994, **36**, 87–92.
6. Dastur, D. K., Mangheni, D. K. and Udani, P. M., *Radiol. Clin. North Am.*, 1995, **33**, 733–752.
7. Gupta, R. K., Pandey, R., Khan, E. M., Mittal, P, Gujral, R. B. and Chhabra, D. K., *Magn. Reson. Imaging*, 1993, **11**, 443–449.
8. Jinkins, J. R., Gupta, R., Chang, K. H. and Carbajal, J. R., *Radiol. Clin. North Am.*, 1995, **33**, 771–786.
9. Gupta, R. K., Kohli, A., Gaur, V., Lal, J. H. and Kishore, J., *Neuroradiology*, 1997, **39**, 699–704.
10. Usenius, J. R., Kauppinen, R. A., Vainio, P. A., Hernesniemi, M. P., Vapalahti, L. A., Palijarvi, S. and Soimakallio, S., *J. Comput. Assist. Tomogr.*, 1994, **18**, 705–713.
11. Gupta, R. K., Poptani, H., Kohli, A., Chhabra, D. K., Sharma, B. and Gujral, R. B., *Indian J. Med. Res.*, 1995, **101**, 19–24.
12. Gupta, R. K., Roy, R., Dev, R., Husain, M., Poptani, H., Pandey, R., Kishore, J. and Bhaduri A. P., *Magn. Reson. Med.*, 1996, **36**, 829–833.
13. Remy, C., Arus, C., Ziegler, A., SamLai, E., Moreno, A., Fur, Y. L. and Decorps, M., *J. Neurochem.*, 1994, **62**, 166–179.
14. Kuesel, A. C., Donnelly, S. M., Halliday, W., Sutherland, G. R. and Smith, I. C. P., *NMR Biomed.*, 1994, **7**, 172–180.
15. Peeling, J. and Sutherland, G., *Magn. Reson. Med.*, 1992, **24**, 123–126.
16. Sze, D. Y. and Jardetzky, D. O., *Biochem. Biophys. Acta*, 1990, **1054**, 198–206.
17. Gobson, G., Minnikin, D. E., Besra, G. S., Mallet, A. I. and Magnusson, M., *Biochem. Biophys. Acta*, 1990, **1042**, 176–181.
18. Bhargava, D. K., Shrinivas, Chawla, T. C., Tandon, B. N. and Kapur, B. M. L., *J. Trop. Med. Hyg.*, 1985, **88**, 249–252.